Aerodynamics and Control of Next Generation Electric Rotorcraft

Graeme Hocking[1] Winston L. Sweatman[2]
Benjamin Maldon[3] Susam Boral[4] Philipp Braun[5]
Hiroaki Kurihara[6] Michael H. Meylan[7] Björn Rüffer[8]
Natalie Thamwattana[9]

2022-03-19

Abstract

Innovative design of helicopters promises great benefits over conventional aircraft but there are a number of technical challenges. Hyper Q Aerospace brought a project to the 2020 Mathematics-in-Industry Study Group to consider a helicopter design with a counter-rotating, coaxial, double rotor. Specific considerations were the vibration and harmonic properties of the rotor blades, the noise from the aircraft and the aerodynamic characteristics. Euler–Bernoulli beam theory and classical airfoil theory were implemented to consider the vibration and aerodynamic features of the aircraft and the rotor system. The fundamental lengthwise and lateral harmonics of the blades were obtained and compared with typical rotational forcing frequencies. The

DOI:10.21914/anziamj.v62.15964, Published 2022-03-19, as part of the Proceedings of the 2020 Mathematics and Statistics in Industry Study Group. ISSN 1445-8810. (Print two pages per sheet of paper.)

modification to the lift generated by the counter-rotating blades and noise mitigation strategies were discussed. Improved design strategies were presented.

Contents

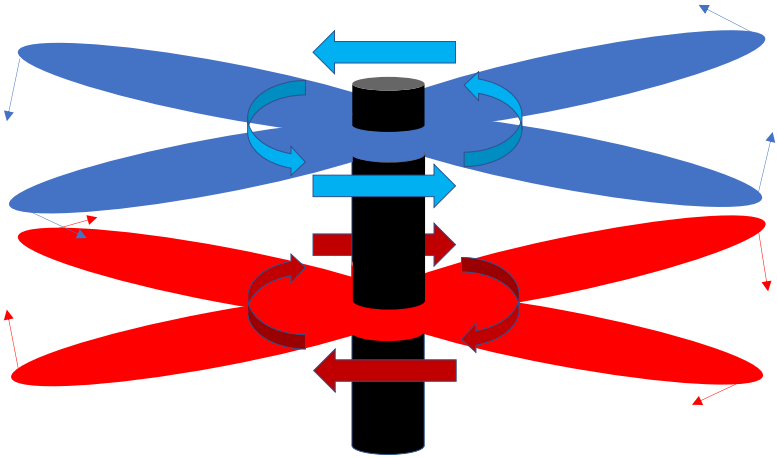

Figure 1: A schematic diagram of the helicopter rotors. The Hyper-Q design has counter-rotating rotors to balance the momentum and remove the necessity for a tail rotor.

1 Introduction

Mathematical modelling of aircraft is challenging because of the complexities of flight. However, at the simplest level, with a solid factual foundation, modelling can provide some insight into the processes involved. This can then be further explored with experimental trials. In this spirit, the 2020 Mathematics-in-Industry Study Group (MISG2020) undertook a study relating to helicopter flight, for the company Hyper Q Aerospace.

The topic of flight has previously appeared at the annual Mathematics-in-Industry Study Group [3]. A 2005 project was inspired by a series of patents from the 1930s. However, in this MISG 2005 project, the lack of technical details and experimental data was challenging in the modelling process, and somewhat constrained progress.

The company Hyper Q Aerospace is developing an aircraft that is powered by a coaxial rotor-head. The counter-rotating rotors will be driven directly by electric axial flux motors, and their compensating angular momentum means that no tail rotor is required (Figure 1). Unlike conventional helicopter design there will be limited requirements for gearboxes, transmissions or drive shafts.

Blade length is approximately 3 m giving a rotor disk size of about 6.5 m, and the rotor disk separation is about 0.5 m. Typical angular velocity of helicopter blades is around 600 RPM, but this model is designed to operate at values 250–1500 RPM. Aircraft velocity will vary from 0 to 300 knots (550 km/hr).

The major factors for consideration by the study group were the vibrations in the system, the noise generated by the new design, and the aerodynamic response. We relate the findings of each in turn. The following questions were identified on the first day of the workshop.

- *Question 1: What are the vibration modes present?*
  - within the blades
  - within the entire rotor system
  - between the rotor disks
  - due to blades crossing
- *Question 2: How is the lift affected by the coaxial design?*
  - What is the lift generated by the two blade system?
  - What is the effect of blade crossing?
- *Question 3: What is the noise footprint?*

2 Critical Frequencies/Harmonics of the Blade

Vibrations are an inevitable occurrence in systems of this type. In general, these vibrations are harmless to the integrity of the craft. However, serious damage may result if there is feedback between components leading to resonance and consequently growing oscillations. Possible sources of vibration are

the blades as their velocity changes, the movement of the entire rotor, and the interaction between the rotor disks and the blades as they cross.

The frequency of all of these sources of vibration are readily determined with the exception of the vibrations of the rotor blades. However, in Section 2.1, we use Euler–Bernoulli beam theory to estimate the vibrations of each rotor blade.

2.1 Euler–Bernoulli Beam Theory

The vibration characteristics of the rotor blades are calculated using the Euler–Bernoulli equation [10]. This equation models the oscillations in a beam of small thickness, simplifying the equations of solid mechanics. So long as the oscillations are relatively small it provides an accurate representation of the behaviour of the beam given the basic material properties. Both along-beam oscillations and across-beam oscillations are considered, and the resonant frequencies and harmonics are computed. The nice thing about this approach is that the solutions are computed quickly, and exactly, given the characteristics of the blade.

The calculation provides the major frequencies within the rotor blades that should be avoided in other components within the rotorcraft, such as the engine vibration, rotor cycling or rotor crossing. If this is not done, and these other components are maintained at the same value of frequency, then the energy within these components may feed into the rotor oscillations causing resonance and ultimately failure. In what follows we compute the frequencies with Euler–Bernoulli beam theory and compare with finite element simulations. These calculations do not account for the rotating frame of reference. Such effects can be considered using the techniques by Yang et al. [12].

2.1.1 Vibration analysis of a single beam/blade

We consider the Euler–Bernoulli equation [10],

$$EI\frac{\partial^4\eta}{\partial x^4} + M\frac{\partial^2\eta}{\partial t^2} = 0 \tag{1}$$

together with the boundary conditions

$$\eta = 0\,, \quad \frac{\partial\eta}{\partial x} = 0 \quad \text{at } x = 0\,, \tag{2}$$

$$\frac{\partial^2\eta}{\partial x^2} = 0\,, \quad \frac{\partial^3\eta}{\partial x^3} = 0 \quad \text{at } x = L_B\,. \tag{3}$$

Here η denotes the displacement (in metres), and this depends on the position on the blade x and on time t. Time variation is considered as a simple harmonic, that is, $e^{-i\omega t}$. The quantity EI is a property of the blades (E is the modulus of elasticity and I is the moment of inertia of the cross-section), and data was provided by Hyper Q Aerospace. L_B denotes the length of the blade/beam (in metres) and M denotes the uniformly distributed mass of the blade/beam (in kg/m). The conditions (2) indicate that the end at $x = 0$ is fixed, whereas the conditions (3) allow for the movement of the free end at $x = L_B$. A general solution of the partial differential equation (1) is

$$\eta(x,t) = [c_1\cosh(Kx) + c_2\sinh(Kx) + c_3\cos(Kx) + c_4\sin(Kx)]\,e^{-i\omega t} \tag{4}$$

for constants c_1, c_2, c_3, c_4. Here, $K \in \mathbb{R}$ denotes a wave number, and ω represents the forcing frequency due to the rotation of the rotor.

A nontrivial solution of the Euler–Bernoulli System (1)–(3) exists when the nonlinear equation

$$1 + \cos(KL_B)\cdot\cosh(KL_B) = 0 \tag{5}$$

is satisfied. Equation (5) has infinitely many solutions K_n, $n \in \mathbb{N}$, from which wave numbers for different harmonics are derived. In particular, for any K_n

Figure 2: Visualization of the first four modes corresponding to the solution (7) for $c_{1n} = 1$ and $L_B = 3.25$. The magnitude of the amplitude depends on the initial conditions. The value used here is solely for illustration.

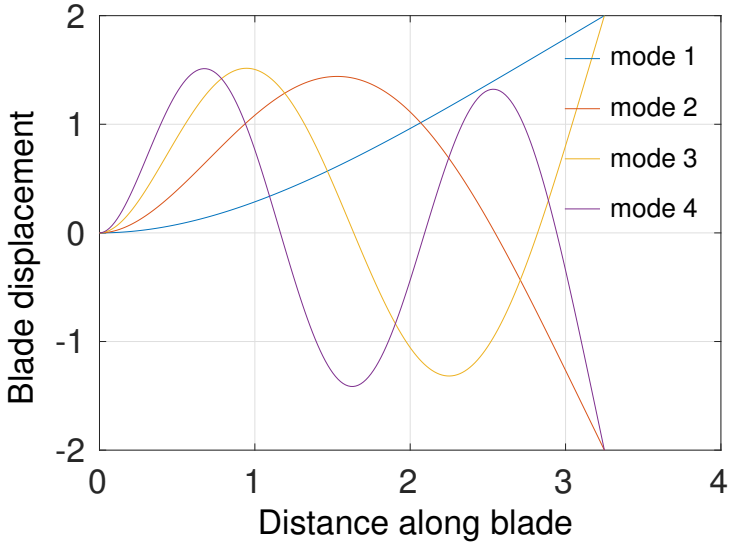

satisfying (5), the corresponding angular frequency of the rotational forcing

$$\omega_n = \sqrt{\frac{EI}{M}} K_n^2 \,. \tag{6}$$

For a fixed K_n, the given boundary conditions lead to the solution

$$\begin{aligned} \eta_n(x) = c_{1n} \Big\{ & [\cosh(K_n x) - \cos(K_n x)] \\ & + \frac{\cos(K_n L_B) + \cosh(K_n L_B)}{\sin(K_n L_B) + \sinh(K_n L_B)} [\sin(K_n x) - \sinh(K_n x)] \Big\}, \end{aligned} \tag{7}$$

with the free constant c_{1n}. The constant c_{1n} is determined from the initial condition. Figure 2 shows the shapes of the first four modes.

Table 1: Lengthwise vibration frequencies (Hz) for calculations at different RPM (Revolutions per minute) for Euler–Bernoulli theory and Finite Element computations.

Mode	Euler–Bernoulli		Finite Element	
	Frequency	RPM	Frequency	RPM
1	1.23	74.	1.36	81.6
2	7.73	463.9	8.72	523.2
3	21.66	1298.8	38.4	2304.
4	42.42	2545.3	80.8	4848.

Table 1 reveals that the first two values of frequency for the lengthwise modes are similar to the finite element simulation data provided by Hyper Q Aerospace. The details of the finite element simulations were not provided by Hyper Q Aerospace, as they are commercial in-confidence.

The third value differs; however, it is possible the third mode is missing, in which case the alignment is quite good. Results indicate that the second and third modes are the most relevant for the Hyper Q Aerospace design.

The comparison of the cross-wise oscillations, seen in Table 2, is less accurate due to the short distances involved, making the results much more susceptible to small variations in the parameters. The results are computed in isolation, rather than as part of the whole blade vibrating (as in the FEM) and as a consequence this difference is to be expected. However, importantly, the cross-wise oscillations are at a much higher frequency and so are of almost no concern to Hyper Q Aerospace (personal communication).

The Euler–Bernoulli theory is quickly deployed to compute variations to the standard design. Here we demonstrate this by considering another mass added at the end of the beam/blade. This analysis is the same as before except for a modification to the free-end shear moment (3) to produce

$$EI\frac{\partial^3\eta}{\partial x^3} = M_1\omega^2\eta(L_B) \quad \text{at } x = L_B\,. \tag{8}$$

Table 2: Crosswise vibration frequencies (Hz) for calculations at different RPM (Revolutions per minute) for Euler–Bernoulli theory and Finite Element computations.

Mode	Euler–Bernoulli		Finite Element	
	Frequency	RPM	Frequency	RPM
1	7.67	460.	6.42	385.2
2	48.08	2885.	24.8	1488.
3	134.63	8078.	48.9	2934.
4	263.82	15829.	100.5	6030.

The general solution (4) remains the same. The boundary conditions lead to the matrix equation

$$\begin{bmatrix} 1 & 0 & 1 & 0 \\ 0 & 1 & 0 & 1 \\ \cosh(KL_B) & \sinh(KL_B) & -\cos(KL_B) & -\sin(KL_B) \\ A & B & C & D \end{bmatrix} \begin{bmatrix} c_1 \\ c_2 \\ c_3 \\ c_4 \end{bmatrix} = \mathbf{0}, \tag{9}$$

and further

$$A = A(K, \omega, M_1, L_B) = \sinh(KL_B) + \frac{M_1\omega^2}{K^3}\cosh(KL_B), \tag{10}$$

$$B = B(K, \omega, M_1, L_B) = \cosh(KL_B) + \frac{M_1\omega^2}{K^3}\sinh(KL_B), \tag{11}$$

$$C = C(K, \omega, M_1, L_B) = \sin(KL_B) + \frac{M_1\omega^2}{K^3}\cos(KL_B), \tag{12}$$

$$D = D(K, \omega, M_1, L_B) = -\cos(KL_B) + \frac{M_1\omega^2}{K^3}\sin(KL_B). \tag{13}$$

A non-trivial solution exists when the determinant of the 4×4 matrix in (9) is zero, and using that relation we derive K_n. Again, as for the lengthwise case, K_n and ω_n are related by equation (6).

Figure 3 shows the first four modes of vibration lengthwise when a 0.5 kg weight is added to the end of the blade. Figure 4 shows the effect of the

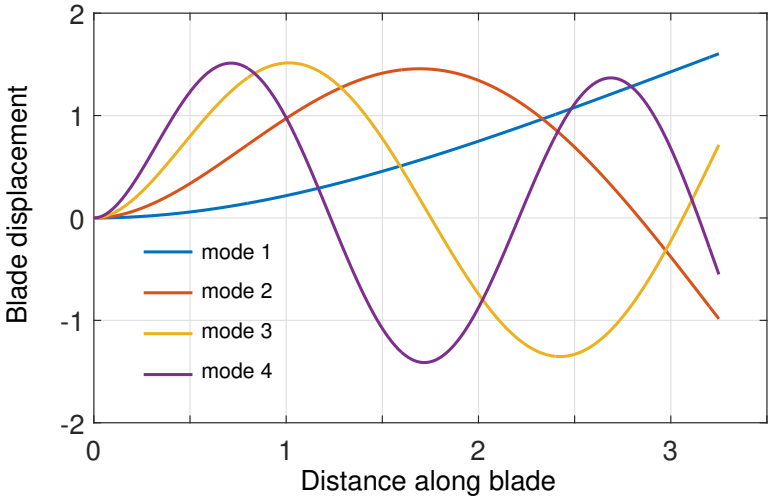

Figure 3: modes of lengthwise oscillation with a 0.5 kg mass added to the end of the blade.

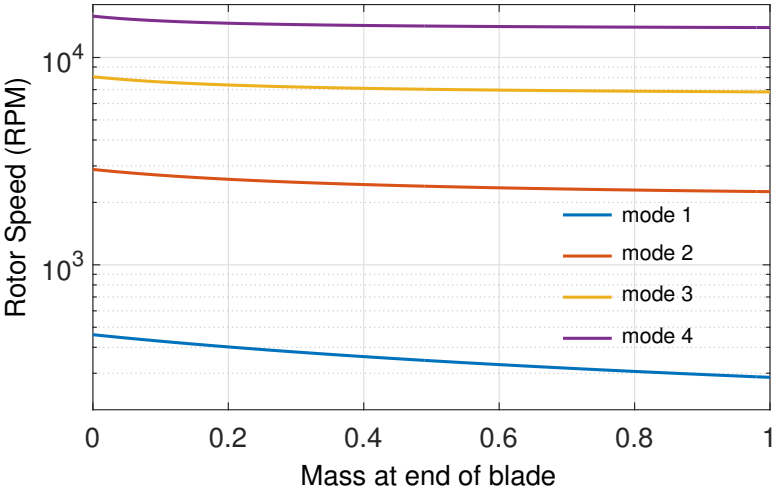

Figure 4: the effect of the mass on the frequency of the critical harmonics. As the load on the end is increased the critical frequency decreases slightly.

weight on the critical frequencies of these four modes. As more weight is added, the critical values reduce slightly.

This section has shown that, given the appropriate data, the important vibration modes can be quickly calculated for any configuration that the manufacturer wishes to deploy. A range of possible configurations can quickly be tested for appropriateness and to ascertain the likelihood of interactions with other components.

3 Aerodynamic Performance

One of the most important components of a helicopter design is the lift generated by the rotors. In the design of Hyper Q Aerospace, there are two counter-rotating blades, rotating at a speed of between 250–1500 RPM. Each blade of a helicopter produces an average lift L, and so the total lift on a single rotor helicopter is estimated by summing over all lifting surfaces. However, the total lift in this two rotor configuration is changed by the interaction of the air from the different blades.

We adopted a staged process in investigating the properties of such a system. Flow past a single airfoil was considered to gain a general understanding of the region-of-influence in the surrounding air and the lift generated. The work of aerodynamics pioneers including application of the Joukowski transformation and thin airfoil theory [2, 5, 6, 9] was used to examine the lift generated by different wing configurations. These classical results, many of which were produced in the early part of the 20th century, provide very accurate and relatively simple computations for lift on a single airfoil of any reasonable single blade profile. The results provide a good approximation to the local flow without the undue complication of a full computational fluid dynamics (CFD) simulation, and also enable some general conclusions to be drawn about the features of the flow and wing shapes. Hyper Q Aerospace indicated that they did not wish for the MISG to conduct full CFD simulations.

To gain some understanding of the impact of the presence of other lifting surfaces in close proximity, we then consider the interactions in the flow past the wings of a bi-plane, since this incorporates some of the features we seek, yet can still be considered in a steady flow context.

However, for a helicopter with coaxial rotors moving in opposite directions the reference frame in which the wing or blade is stationary and the air flows past is not applicable because the problem is changing with time (unsteady). In order to be able to investigate lift and air pressure, we are interested in finding the streamlines as the blades of the counter-rotating airfoil discs pass each other. Finally, we attempt to infer the resulting behaviour by what we learnt from these relatively simple calculations.

The traditional approach in aerodynamics is to assume steady, irrotational flow of an inviscid, incompressible fluid, in which case the problem to solve for flow past an object is to find a velocity potential, $\phi(x, y)$, that satisfies

$$\nabla^2 \phi = 0 \quad \text{on } \Theta, \tag{14}$$

$$\nabla \phi \cdot \vec{n} = 0 \quad \text{on } \partial\Theta, \tag{15}$$

$$\nabla \phi \to \vec{U} \quad \text{as } (x, y) \to \infty, \tag{16}$$

where Θ is the fluid domain, $\vec{n}$ is the outward normal to the surface, $\partial\Theta$, of all bodies in the flow, and $\vec{U}$ is the velocity of the free air stream. The velocity potential is used to obtain the horizontal velocity component as $u = \phi_x$ and the vertical component as $v = \phi_y$. Condition (15) represents that the air cannot pass through the surface of the body, whereas (16) ensures that the air flow should approach the free-stream value, $\vec{U}$ as the distance from the wing increases.

3.1 A single airfoil

We begin with a study of flow past a single airfoil. One method that provides a deep understanding of such flows involves the use of the famous "Joukowski"

transformation [5, 7] and this method is used to consider some general features of the flow. In this technique, the flow past a circular cylinder is transformed into flow past a vast range of airfoil shapes, both symmetric and cambered, using complex-variable theory in two dimensions. The assumption of two-dimensional flow means that the theory does not consider end effects, but it does highlight the main factors affecting the flow and generating the lift. Section 3.1.4 considers what is known as thin-airfoil theory as this can be extended to a configuration with two wings, such as in a bi-plane. This enables us to consider the impact of the second lifting surface.

3.1.1 Joukowski map

The important feature of this method [5, 7] is the mapping of the shape of a circle into an airfoil shape using conformal mapping. We demonstrate how this transformation modifies a cylinder to a symmetric or cambered airfoil, although for simplicity we only do computations for a symmetric case. Once this transformation is known for a particular shape, then the flow is computed. Consider a circle of radius $1+\varepsilon$ centred at $(-\varepsilon, 0)$ in the complex $z = x + iy$ plane (where $i = \sqrt{-1}$). The mapping

$$f(z) = \frac{z}{2} + \frac{1}{2z}\,. \tag{17}$$

takes this circle in the z-plane to a symmetric airfoil in the f-plane. Since the equation for flow past a cylinder is known, we transform this flow to that past any object mapped under this transformation. Figure 5 shows the result for the mapping for the case where $\varepsilon = 0.3$. If the circle is symmetric about the horizontal axis, then the resulting airfoil is symmetric. Therefore, to introduce a camber to the airfoil, we vertically offset the centre of the circle to be $(-\varepsilon, \delta)$ for some small positive δ. Figure 6 shows an airfoil for $\varepsilon = 0.3$ and $\delta = 0.1$.

As an example, we consider the standard *NACA0012 airfoil*. The numbers indicate the shape of the airfoil; the first two digits give the amount and

Figure 5: The result of a transformation of a circle of radius 1.3 and centre $(-0.3, 0)$ under the Joukowski map, for the case with $\varepsilon = 0.3$.

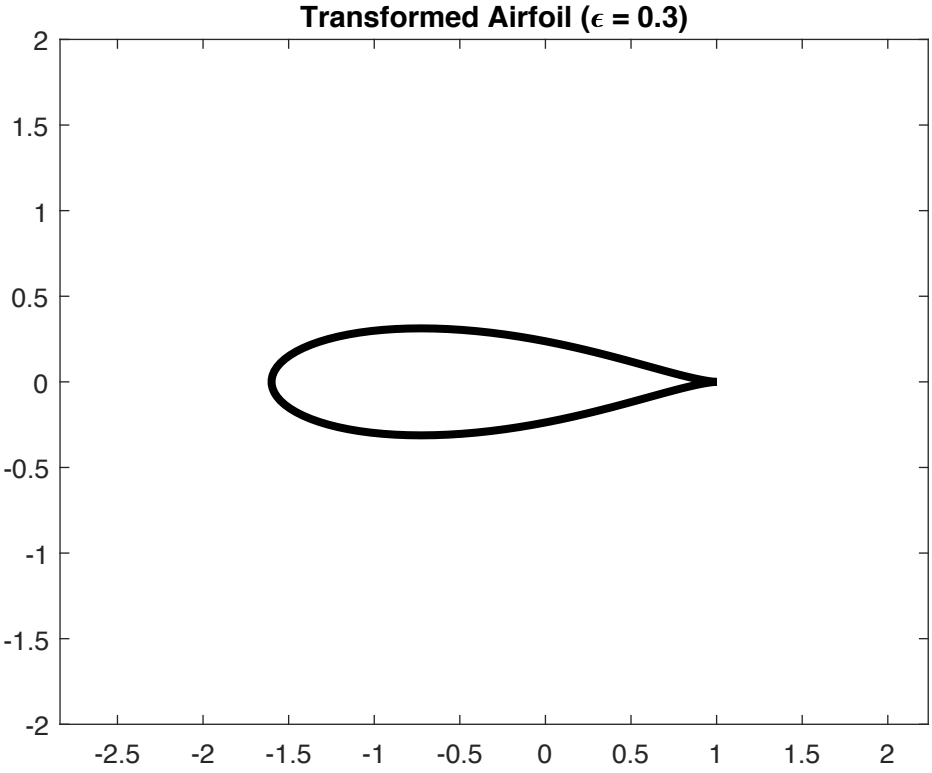

location of the camber, whereas the last two indicate the maximum thickness as a percentage of the chord length. Thus, this is a symmetric airfoil in which the maximum thickness is 0.12 times the chord. This is not typical of a helicopter blade for which the ratio is much larger. Importantly, typical helicopter blades are thinner than this, but these calculations are for demonstration purposes only. In order to consider the flow past this shape, we must choose ε so that the resultant airfoil has the maximum thickness of $h = 0.12$ of the chord, c.

Figure 6: The result of a Joukowski transformation of a circle of radius 1.3 and centre $(-0.3, 0)$ for the case with $\varepsilon = 0.3$ and $\delta = 0.1$, introducing a camber to the shape.

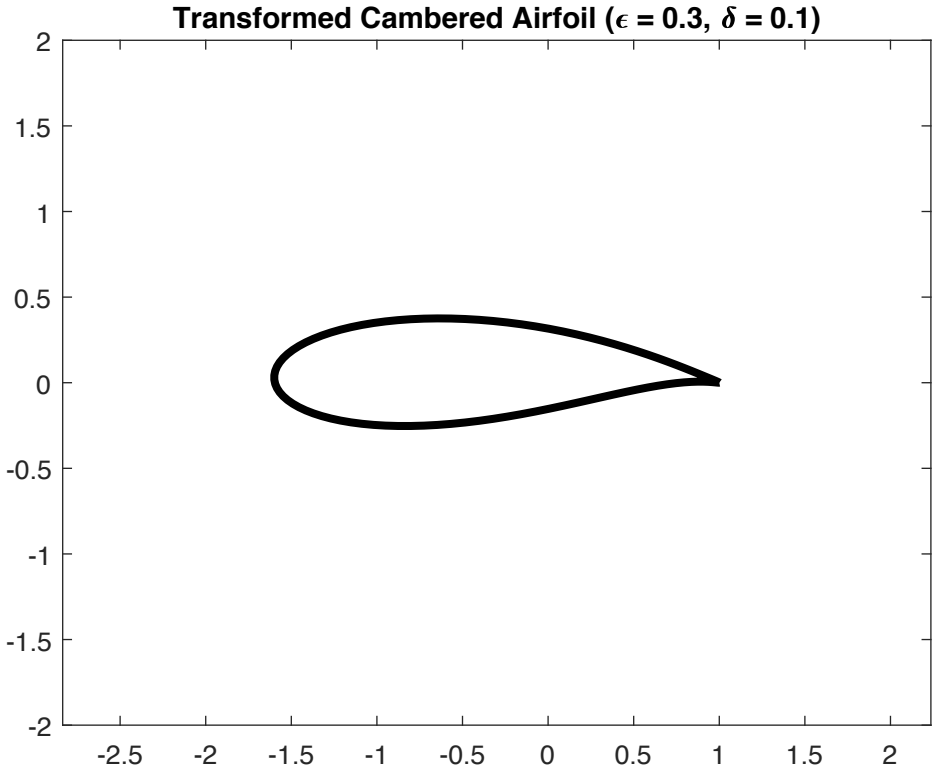

The width of the chord line, as dependent on ε, is

$$c(\varepsilon) = |f(1) - f(-2\varepsilon - 1)| = \frac{2(\varepsilon+1)^2}{2\varepsilon+1}. \tag{18}$$

Likewise, the thickness is dependent on ε via

$$h(\varepsilon) = \left|f[\varepsilon + (\varepsilon+1)i] - f[\varepsilon - (\varepsilon+1)i]\right| = \frac{2\varepsilon(\varepsilon+1)^2}{\varepsilon^2 + (\varepsilon+1)^2}. \tag{19}$$

The thickness ratio, defined as $A_T = h/c$, is

$$A_T(\varepsilon) = \frac{h(\varepsilon)}{c(\varepsilon)} = \frac{\varepsilon(2\varepsilon+1)}{\varepsilon^2 + (\varepsilon+1)^2}. \tag{20}$$

Solving for ε, we find the positive solution is

$$\varepsilon = \frac{-2A_T + 1 - \sqrt{-4A_T^2 + 4A_T + 1}}{4(A_T - 1)}. \tag{21}$$

For $A_T = 0.12$, we find $\varepsilon \approx 0.123$. Figure 7 is a plot of this symmetric airfoil using the Joukowski map.

3.1.2 Airstream

In complex variables, the most general equation for the complex potential for flow past a cylinder, with centre $(-\varepsilon, 0)$ and radius $R = 1 + \varepsilon$, is

$$G(z) = \phi(x,y) + i\psi(x,y) = U\left[z + \frac{(\varepsilon+1)^2}{z+\varepsilon}\right] - i\Gamma \log(z+\varepsilon), \tag{22}$$

where U is the speed of the free air stream and $z = x + iy$. The real part, $\phi(x,y)$, is the velocity potential and the imaginary part, $\psi(x,y)$, is known as the streamfunction. As an analytic function, the real and imaginary parts satisfy Laplace's equation (14). The derivative of the velocity potential

Figure 7: The NACA0012 airfoil represented by the image of a Joukowski map with $\varepsilon = 0.123$.

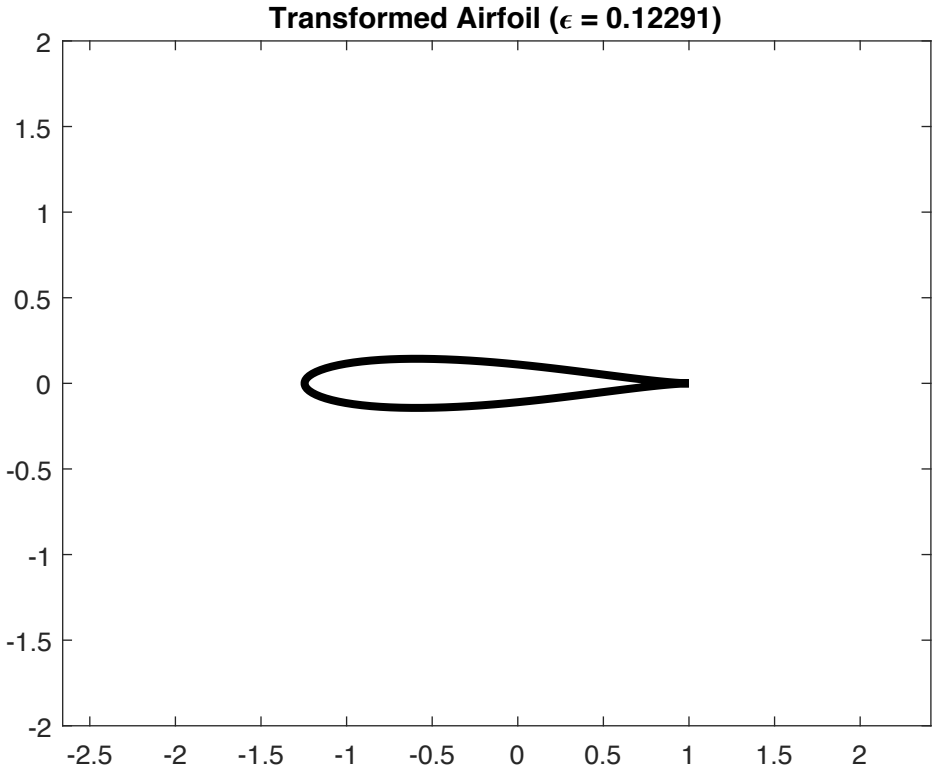

provides the velocity field, $f'(z) = u - iv = \phi_x - i\phi_y$ of the air. The streamfunction has the property that in steady flow the air flows along lines for which the value of the streamfunction is constant (called *streamlines*). The second, log term is a circular flow, called a vortex, situated at the centre of the circle. The quantity Γ is called the circulation and represents a "rotating" flow around the circle. For flow past an object, the inclusion of this term represents an infinite number of possible solutions via different values of Γ. This non-uniqueness is resolved by what is known as the "Kutta-condition" [6, 9], that

stipulates that, for a wing with an aerodynamic tail in normal flight, the flow will separate smoothly from the trailing edge. It turns out that lift on the wing is directly proportional to the value of Γ, via the relation

$$L = \rho U \Gamma, \tag{23}$$

where ρ is air density. The top plot of Figure 8 shows the streamlines of this solution for flow past a cylinder and the bottom plot shows the corresponding streamlines for flow past the airfoil shown in Figure 7. We see that airstreams are affected further away from the cylinder than for the airfoil, as expected due to the smoothness of the surface and separation. In this example, due to the symmetry and that there is zero angle of attack, the value of $\Gamma = 0$ and there is no lift on the wing.

Although the air is disturbed around the airfoil, it is only over a relatively small region, not much more than the length of the airfoil.

3.1.3 Angle of Attack Considerations

In the case of a symmetric airfoil, the only way to generate lift in open air is to tilt the airfoil slightly upward into the oncoming flow. This tilting is called the "angle of attack" and leads to an asymmetry in the flow causing the pressure above the airfoil to decrease as the relative air speed increases, and the pressure below to increase, due to a slightly lesser increase in speed. It is the difference in pressure above and below the wing that causes the lift.

As the angle of attack α for an airfoil increases, the airstreams are also affected. It is convenient to rotate the airstream slightly rather than the airfoil, giving the modified potential

$$G(z) = U\left[ze^{-i\alpha} + e^{i\alpha}\frac{(\varepsilon+1)^2}{z+\varepsilon}\right] - i\Gamma\log(z+\varepsilon). \tag{24}$$

To satisfy the Kutta condition, the velocity of the airstream at the point on the sphere that maps to the tail of the airfoil under the transformation must

Figure 8: Plot of the airstreams about a cylinder (top) and the flow past the transformed shape after the Joukowski map (bottom). The angle of attack is zero and the objects are symmetric, so no lift is generated on either shape.

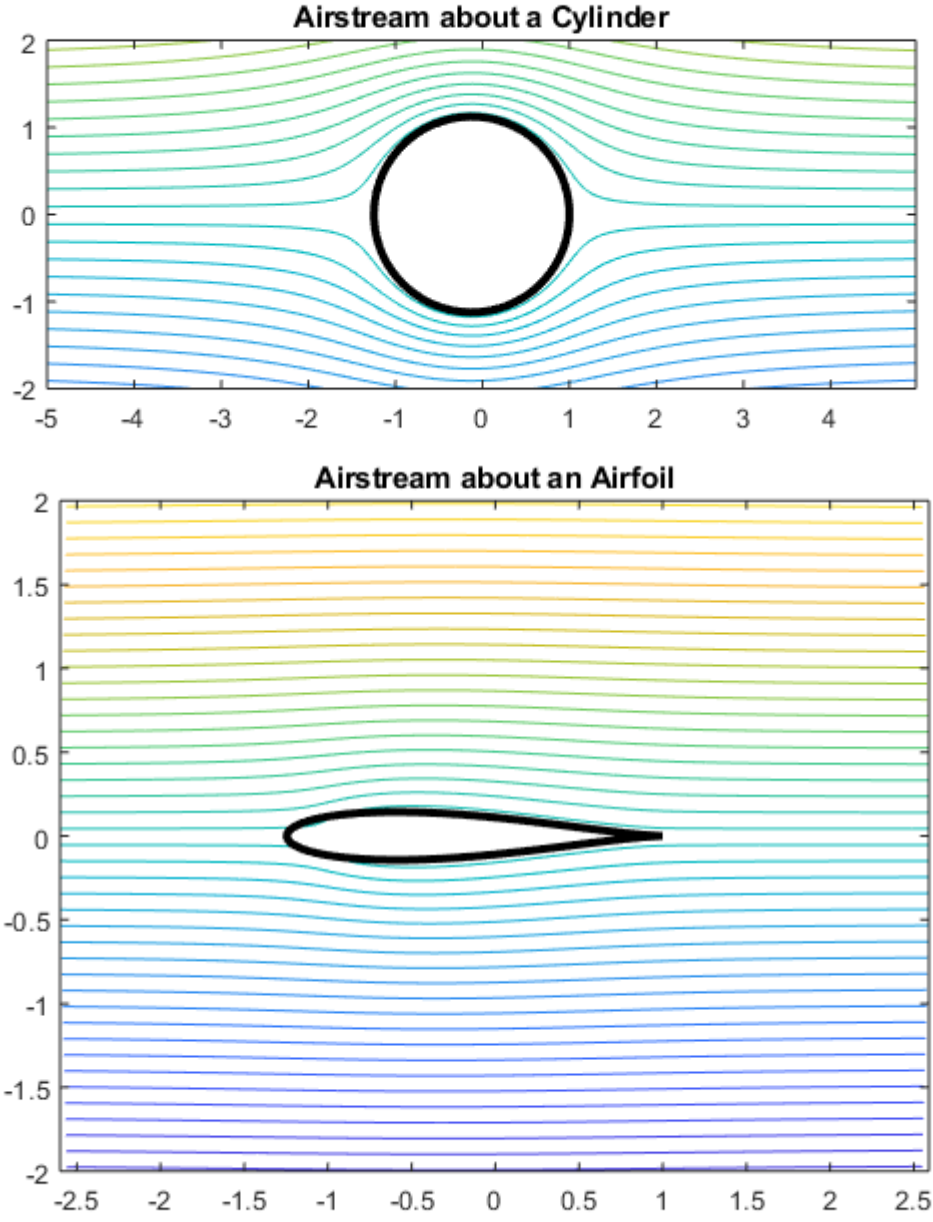

be zero, ensuring that the separation from the tail is smooth. Thus for a given angle of attack α,

$$\left.\frac{dG}{dz}\right|_{z=1} = 0 \implies \Gamma = -2U(\varepsilon + 1)\sin(\alpha). \tag{25}$$

For small angles of attack, $\sin\alpha \approx \alpha$, and so the relation between angle of attack and lift is almost linear. Typically, to avoid stall (and the separation of the boundary layer and loss of lift), $\alpha < 10°$. The airstream computed with (24) is shown in Figure 9. The separation from the trailing edge is smooth. Once the air has passed the airfoil it resumes its travel at angle α.

3.1.4 Thin Airfoil Theory

One of the oldest theories for lifting surfaces is known as thin-airfoil theory [6, 1]. It is more general than Joukowski transforms and has the advantage of providing some nice "rules of thumb" about lifting surfaces. It is a very powerful approach that allows for analytical calculations of lift for a number of different shapes predicated on wings generally being very thin. Given this assumption, everything is expanded about the line $y = 0$ in two dimensions. The wing is assumed to lie along $-l < x < l$, where the chord length $c = 2l$, and an expansion is performed about $y = 0$ to compute variations for angle of attack and curvature. The potential $\phi = Ux + \mathcal{O}(\varepsilon^2)$ is broken up into odd and even components, where ε is the ratio of wing thickness to chord of the wing and U is the velocity. By symmetry the even component cannot contribute to the lift on a single airfoil, and so it remains to solve for the odd component. Setting $\phi = Ux + \Phi$, the problem becomes

$$\nabla^2\Phi = 0, \tag{26}$$
$$\Phi_y = Uf_x^{\pm} \quad \text{on } y = 0^{\pm}, \text{ for } -l < x < l, \tag{27}$$
$$\Phi \to 0 \quad \text{as } (x, y) \to \infty, \tag{28}$$

Figure 9: Plot of the airstream for the NACA0012 airfoil at angle of attack $\alpha = 10°$. The circulation value for this example is $\Gamma \approx -0.39$, computed from (25).

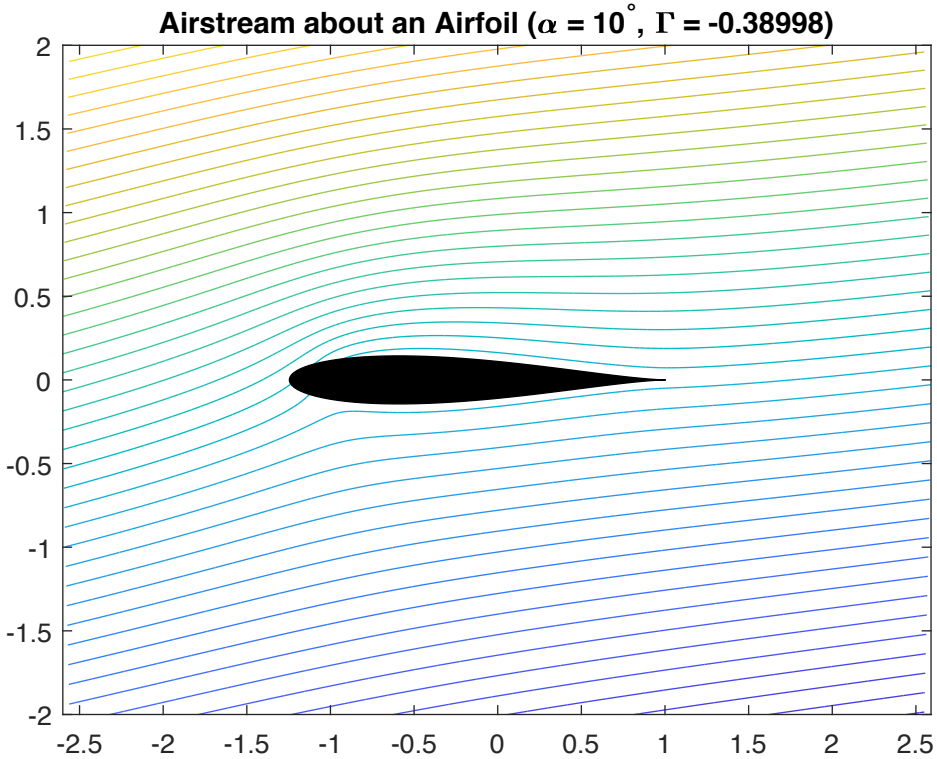

where $f^{\pm}(x)$ are the upper and lower surface of the wing and $\bar{f}(x) = (f^{+}(x) + f^{-}(x))/2$ is the centreline of the wing. A solution is obtained by using a vortex distribution along the wing, that is,

$$\Phi(x, y) = -\frac{1}{2\pi}\int_{-l}^{l} \gamma(\xi) \arctan\left(\frac{y}{\xi - x}\right) d\xi\,. \tag{29}$$

If $(x, y) \to \infty$, then $\Phi(x, y) \to \frac{\Gamma}{2\pi}\arctan(y/x)$, where $\Gamma = \int_{-l}^{l}\gamma(\xi)d\xi$ is the total vortex strength, effectively the circulation, and then the lift per unit span is $-\rho U\Gamma$. Making the appropriate substitutions, the problem becomes a singular, first-kind integral equation for the vortex strength $\gamma(x)$,

$$\frac{1}{\pi}\int_{-l}^{l} \frac{\gamma(\xi)}{x - \xi}\, d\xi = 2U\bar{f}'(x). \tag{30}$$

This is solved as

$$\gamma = \gamma_0(x) + \frac{\Gamma}{2\pi}(l^2 - x^2)^{-1/2}, \tag{31}$$

where the second term is a solution to the homogeneous form of the integral equation (30), and

$$\gamma_0(x) = -\frac{(l^2 - x^2)^{-1/2}}{\pi}\int_{-l}^{l} \frac{(l^2 - \xi^2)^{1/2} 2U\bar{f}'(\xi)}{x - \xi}\, d\xi \tag{32}$$

is the particular solution [11]. This ultimately gives an expression for the total vortex strength for any thin airfoil shape of

$$\Gamma = 2U\int_{-l}^{l} \sqrt{\frac{l + \xi}{l - \xi}}\bar{f}'(\xi)\, d\xi\,. \tag{33}$$

The value of Γ must be chosen to ensure that the velocity at the trailing edge is finite. This Kutta condition is the determining factor in the computation of Γ and hence the lift.

As a simple example, the theory solves for a flat plate at an angle of attack α, giving $L = 2\pi \sin\alpha \rho U^2 l$ for the lift. From equation (33), that lift L is a

weighted average of the local angle of attack, where the weight function is $\sqrt{(l+x)/(l-x)}$, which is largest as x approaches l, the trailing edge. Therefore, to maximize the lift on a single airfoil it is better to have a larger angle of attack, but to concentrate it locally near to the trailing edge. Thus wings with camber are more efficient.

This method is used to estimate the lift on a blade at any angle of attack and at any air speed. However, the interaction effect from other blades is not present in these calculations. One approach to study what the effect of another blade might be, is to consider a second blade nearby, such as in a bi-plane configuration. This has the advantage that we are still able to consider the flow as steady, which is mathematically much easier. However, these are very complicated calculations, and so, in Section 3.2, we also demonstrate a different, reasonably simple, numerical approach to compute the lift and interaction between two blades.

3.2 Bi-plane calculation

We assume that the actual direction of travel of the blades with respect to each other has little significance, or that transient effects are minimal, and consider flow past two airfoils, such as in a bi-plane, to try to ascertain the effect on lift.

A similar theory to thin airfoil theory is followed for a biplane by incorporating a second "plate". The theory requires a complex mapping procedure to an alternative complex plane in which the two "wings" are aligned along the axes, and it is then possible again to satisfy the Kutta condition. The details are rather complicated as detailed by Munk [8].

Ultimately, the equation for the lift is

$$L = 4\pi\rho U^2 l \left(B \sin\alpha + \sqrt{B} \sin\alpha_0 \right), \tag{34}$$

where B is a rather complicated constant that represents the separation

between the wings and α_0 is the angle of attack for which the cambered wing has zero lift. In the case of a symmetric wing (no camber), $\alpha_0 = 0$. In general, B is substantially less than one, but as the wings get further apart $B \to 1$ and so the lift approaches that of two separate wings. If the wings get close together then the lift of the combined wings is less than the lift on the two wings as monoplanes. This is known as the biplane effect. Thus $1 - B$ represents the decrease in lift due to the angle of attack and $1 - \sqrt{B}$ that due to the curvature. Therefore, the reduction in lift due to angle of attack is greater than that due to camber in the bi-plane configuration. At the same time, it is possible to compute the repulsive force and the induced drag between the two wings [8, 9].

This theory assumes the two wings are vertically aligned (no stagger), but is modified by Munk [8] to include vertical stagger and thus the changes in lift experienced if the two wings are vertically offset. Since, in potential flow, the fundamental equation has no explicit dependence on time, this would provide a first estimate of how the blades interact as they pass each other.

3.2.1 A numerical approach

We compute the flow past any number of objects using a numerical scheme based on fundamental solutions to Laplace's equation (14). The linearity of the equation allows us to take a linear combination of known solutions. Thus we make this ansatz,

$$\phi = Ux + \sum_{j=1}^{N} \left\{ \frac{\Gamma_j}{2\pi} \arctan \frac{y - y_{cj}}{x - x_{cj}} + \sum_{k=1}^{n} m_{jk} \log \left[(x - x_{jk})^2 + (y - y_{jk})^2 \right]^{1/2} \right\} \tag{35}$$

where (x_{jk}, y_{jk}) are n interior points of the N airfoils, Figure 10, representing sources and sinks, and (x_{cj}, y_{cj}), $j = 1, \ldots, N$, are appropriately chosen points within each of the wings. In a bi-plane configuration, $N = 2$. The sources (m_{jk} with positive sign) and sinks (m_{jk} with negative sign) need to

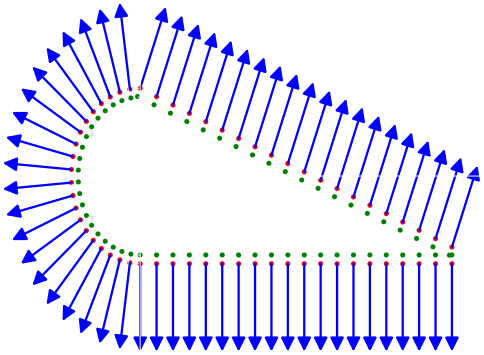

Figure 10: An airfoil blade made up of sources and sinks (green points). The boundary condition (15) is enforced at the red points so that there can be no flow through the surface of the airfoil. The blue arrows represent the normal vectors $\vec{n}$.

be balanced to close off each of the bodies, which imposes the conditions

$$\sum_{k=1}^{n} m_{jk} = 0 \quad \text{for } j = 1, \ldots, N. \tag{36}$$

The Ux term in equation (35) describes the mean horizontal flow that the blades encounter. In equation (36), the weights m_{jk}, $k = 1, \ldots, n$, $j = 1, \ldots, N$, are unknown and have to be found numerically to satisfy the boundary condition (15) at n boundary points. Together with equation (36) we obtain a linear system of equations for the vector of unknown coefficients. The final step is the choice of Γ_j, $j = 1, \ldots, N$, that ensures the smooth separation from the trailing edges, but this is a very difficult calculation.

Once the coefficients are known, we plot the contours of the velocity potential function (35). These contour lines, for the case of a bi-plane, $N = 2$, are shown in the left panel of Figure 11 for $\Gamma_1 = \Gamma_2 = 0$ and are perpendicular to the streamlines, shown in the right panel of Figure 11. Unfortunately, it is quite difficult to satisfy the Kutta condition to determine the circulation and hence the lift and so these calculations were not completed during the time of the study group.

Figure 11: Contour plot of the velocity potential function ϕ (left panel) and the resulting streamlines.

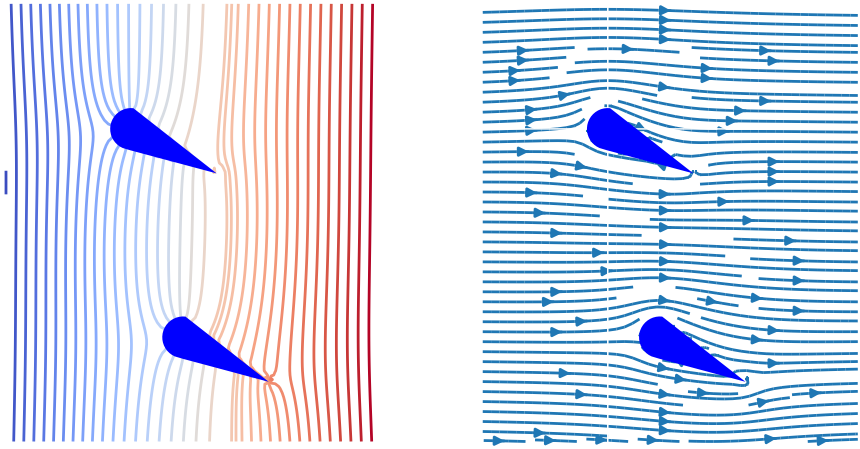

3.3 Other factors

Bi-planes are generally accepted to produce about 1.4 times the lift of a single wing aircraft. So although there is extra lift in comparison, the bi-plane does not provide as much lift as that due to two separate single wings.

The full problem of determining the air flow for counter-rotating blades is very difficult but, after considering what had been learned during the week, the group felt that some general conclusions could be drawn. When the blades pass over and under one another the two interact in a manner that can be thought of as a "ground effect". Ground effect is the increase in lift on an airfoil caused by the distortion of the air flow by the proximity of the ground (or in this case the other blade). The ground effect on the upper blade due to the lower blade increases its lift due to an increase in pressure beneath. However, this pressure increase above the lower blade reduces the lift on that blade. To some extent these effects will cancel during a hover,

while when moving forward the blade that is moving toward the direction of travel will experience the greatest change. It seems likely that with the extra impact of induced drag between the rotor blades, there will be some loss of the total lift generated. If there are the same number of evenly spaced blades on each rotor, then all of the blade crossings coincide and the effect occurs simultaneously. If the upper and lower rotor blade numbers are co-prime, then the blade crossings all occur separately, perhaps producing a smoother lift profile during a single revolution.

4 Noise Footprint

The noise generated by a helicopter was considered via a literature search. The findings indicate that most of the noise comes from only a few sources. One source is the rotor itself. There is also the interaction of the rotor with the tail-rotor (on a single main rotor aircraft), engine noise and other mechanical noise. The largest components of the noise are in the lower frequency sounds generated by the rotor itself.

In the design of the Hyper-Q Aerospace helicopter, much of the higher frequency noise will not occur due to the nature of the electric motor, the lack of a tail rotor and the direct drive on the blade system. The lower frequency noise will come from the overlapping of the counter-rotating blades.

There is an exhaustive treatment of helicopter noise in the textbook by Johnson [4]. In summary, if the number of blades in the rotor disc is N and the rotor rotational speed or angular velocity is Ω [radians s^{-1}], then the textbook notes that the noise is usually around the harmonics of the blade crossing frequency, which is $N\Omega$. The largest component of noise therefore has period $T_P = 2\pi/N\Omega$.

For a coaxial system, with rotor discs of N and M blades, respectively, and assuming both discs counter-rotate at the same angular velocity, there will be $2NM$ blade rendezvous per full revolution. If $N = M$, and both discs are

such that the blades are symmetrically arranged, then these rendezvous will align, which leads to a significant increase in rotor noise.

However, another possibility is to select the second rotor disc with a different number of blades, and to choose N and M to be co-prime. In this case, assuming an asymmetric blade arrangement, the 2NM rendezvous will all occur at different times, thus reducing the noise footprint. An even more extreme approach is to replace one rotor by rotating weights to counter the imbalance in angular momentum and avoid the problem of crossing blades.

5 Final Comments

The study group considered several factors in the design of the helicopter. Some general conclusions should be of use.

- Euler–Bernoulli beam theory provides a good estimate of the lengthwise vibration modes in the rotor blades, and can be implemented quite easily to compare with other vibration modes in the aircraft. Results indicate it is the second and third modes that are most important.
- Aerodynamic analysis shows that lift on blades is generated by angle of attack and camber. Thin airfoil theory shows that camber toward the rear of the blade has the most impact on generating lift.
- Lift on a biplane provides some indicators of the lift on the blades of the twin rotor as they overlap, and demonstrates that the total lift is less than the combined lift of the two blades separately.
- The reduction in lift on a bi-plane is less if the blades are further apart, also reducing their repulsive force (which is likely to impact on both vibration and noise). In a bi-plane, the reduction in lift as the two wings get closer in cambered wings is less than the loss in lift due to angle of attack.

- Noise generation comes mainly from the rotor crossings and so contemplation of how the two rotors are configured would be very worthwhile.

This is a very interesting problem and it is clear that much more work could be done to develop the models considered here. It is beyond the scope of this study to consider these factors, but this work provides some important pointers for future work.

Acknowledgements We are grateful to Hyper Q Aerospace for bringing this problem to MISG 2020 and to the industry representatives Peter Batten and Jim Azar. We also acknowledge Jim Hill and Ian Pettet for their contributions to the project group. The organisation and hospitality at University of Newcastle was greatly appreciated.

References

[1] Batchelor, G.K. (1967) *An Introduction to Fluid Dynamics.* Cambridge UP, Cambridge. doi: 10.1002/aic.690140203. M61

[2] Glauert, H (1926) *The elements of Airfoil and Airscrew Theory*, Cambridge University Press, ISBN: 0-521-27494 M52

[3] Hocking, G.C., Stokes,Y.M., Sweatman, W.L. (2005) "Implementing Lanier's patents for stable, safe and economical ultra-short wing Vacu- and Para-planes." In Wake, G.C. (ed.) *Proceedings of the 2005 Mathematics-in-Industry Study Group*, pp. 119–141 (2005) ISBN:0-473-10423-7 M44

[4] Johnson, W. (2013) *Rotorcraft Aerodynamics*, Cambridge University Press, Cambridge,
ISBN: 978-1-107-02807-4, doi: 10.1017/CBO9781139235655 M68

[5] Joukowsky, N. E. (1910) “Aber die Konturen der Tragflächen der Drachenflieger” (on the shapes of the lifting surfaces of kites). Zeitschrift für Flugtechnik und Motorluftschiffahrt (in German). 1: 281-284 and (1912) 3: 81–86. M52, M54

[6] Kutta, W.M. (1902) “Auftriebskräfte in strömenden Flüssigkeiten” (Forces in flowing fluids). Illustr. Aeron. Mitt. 6, 133–135 M52, M58, M61

[7] Milne-Thomson, L.M. (1973) *Theoretical aerodynamics* (4th ed.). Dover Publ. pp. 128–131. ISBN 0-486-61980-X. M54

[8] Munk, M. (1923) *General Biplane Theory*, National Advisory Committee for Aeronautics, Report No. 151. M64, M65

[9] Prandtl, L and Tietjens, O.G. (1957) *Applied Hydro- and Aeromechanics*, Dover, New York. (Translated by J.P. Den Hartog) ISBN-13: 978-0486603759 M52, M58, M65

[10] Timoshenko, S. (1953) *History of strength of materials*, McGraw-Hill, New York, ISBN: 9780486611877 M46, M47

[11] Tricomi, F.G. Integral Equations (Interscience, 1957), ISBN-13-978-0486648286 M63

[12] Yang, J.B, Jiang, L.J., Chen, D.C.H (2004), “Dynamic modelling and control of a rotating Euler–Bernoulli beam", *J. Sound and Vibration*, 274, 863–875. doi: 10.1016/S0022-460X(03)00611-4 M46

Author addresses

1. **Graeme Hocking**, Murdoch University, Australia.
mailto:g.hocking@murdoch.edu.au
2. **Winston L. Sweatman**, Massey University, New Zealand.
mailto:w.sweatman@massey.ac.nz

3. **Benjamin Maldon**, University of Newcastle, AUSTRALIA.
mailto:Benjamin.Maldon@uon.edu.au
4. **Susam Boral**, IIT Kharagpur, INDIA.
5. **Philipp Braun**, Australian National University, AUSTRALIA.
6. **Hiroaki Kurihara**, Kyushu University, JAPAN.
7. **Michael H. Meylan**, University of Newcastle, AUSTRALIA.
8. **Björn Rüffer**, University of Newcastle, AUSTRALIA.
9. **Natalie Thamwattana**, University of Newcastle, AUSTRALIA.